Fast nonadiabatic two-qubit gates for the Kane quantum computer

Charles D. Hill[1,*] and Hsi-Sheng Goan[2,†]
[1]*Centre for Quantum Computer Technology, and Department of Physics, The University of Queensland, St. Lucia, Queensland 4072, Australia*
[2]*Centre for Quantum Computer Technology, University of New South Wales, Sydney, New South Wales 2052, Australia*
(Received 29 January 2003; revised manuscript received 8 May 2003; published 22 July 2003)

In this paper, we apply the canonical decomposition of two-qubit unitaries to find pulse schemes to control the proposed Kane quantum computer. We explicitly find pulse sequences for the controlled-NOT, swap, square root of swap, and controlled *Z* rotations. We analyze the speed and fidelity of these gates, both of which compare favorably to existing schemes. The pulse sequences presented in this paper are theoretically faster, with higher fidelity, and simpler. Any two-qubit gate may be easily found and implemented using similar pulse sequences. Numerical simulation is used to verify the accuracy of each pulse scheme.

DOI: 10.1103/PhysRevA.68.012321 PACS number(s): 03.67.Lx

I. INTRODUCTION

The advent of quantum algorithms [1,2] that can outperform the best known classical algorithms has inspired many different proposals for a practical quantum computer [3–9]. One of the most promising proposals, was presented by Kane [9]. In this proposal, a solid-state quantum computer based on the nuclear spins of ^{31}P atoms was suggested. Although initially difficult to fabricate, this scheme has several advantages over rival schemes [3–8]. These include the comparatively long decoherence times of the ^{31}P nuclear and electron spins [10–17], the similarity to existing Si fabrication technology, and the ability to scale.

There have been two main proposals for pulse sequences to implement a CNOT (controlled-NOT) gate on the Kane quantum computer. In the initial proposal [9], an adiabatic CNOT gate was suggested. Since that time the details of this gate have been investigated and optimized [18–21]. This adiabatic scheme takes a total time of $\approx 26\ \mu$s and has a systematic error of $\approx 5\times 10^{-5}$ [19]. As good as these results are, nonadiabatic gates have the potential to be faster with higher fidelity and allow advanced techniques such as composite rotations and modified rf pulses [22,23].

Wellard *et al.* [24] proposed a nonadiabatic pulse scheme for the CNOT and swap gates. They present a CNOT gate that takes a total time of $\approx 80\ \mu$s with an error [as defined later in Eq. (91)] of $\approx 4\times 10^{-4}$. Although this gate is nonadiabatic, it is slower than its adiabatic counterpart. For the nonadiabatic swap gate, a total time was calculated of 192 μs.

One of the most useful tools in considering two-qubit unitary interactions is the canonical decomposition [25–27]. This decomposition expresses any two-qubit gate as a product of single-qubit rotations and a simple interaction content. The interaction content can be expressed using just three parameters. In the limit that single-qubit rotations take negligible time (in comparison to the speed of interaction), this decomposition can be used to find optimal schemes [26,27], and of particular inspiration to this paper is an almost optimal systematic method to construct the CNOT gate [28].

It is not possible to apply those optimal schemes [26,27] directly to the Kane quantum computing architecture. They assume single-qubit gates take negligible time in comparison with two-qubit interactions, whereas on the Kane architecture, they do not. Second, in the proposal for the Kane computer, adjacent nuclei are coupled via the exchange and hyperfine interactions through the electrons, rather than directly, and so we have a four-''qubit'' system (two electrons and two nuclei) rather than a two-qubit system. Although we cannot apply *optimal* schemes directly, in this paper we use the canonical decomposition to simplify two-qubit gate design.

Apart from being simple to design and understand, gates described in this paper have many desirable features. Some features of these gates are the following.

(1) They are simpler, with higher fidelity, and faster than existing proposals.

(2) They do not require sophisticated pulse shapes, such as are envisioned in the adiabatic scheme, to implement.

(3) *Any* two-qubit gate can be implemented directly using similar schemes. This allows us to implement gates directly rather than as a series of CNOT gates and single-qubit rotations.

This paper is organized as follows. Section II gives an overview of the Kane quantum computer architecture and single-qubit rotations. Section III describes the canonical decomposition as it applies to the Kane quantum computer. Section IV describes pulse schemes for control Z gates and CNOT gates. Section V gives potential pulse schemes for swap and square root of swap gates. Finally, the conclusion, Section VI, summarizes the findings of this paper.

II. THE KANE QUANTUM COMPUTER

A. The Kane architecture

A schematic diagram of the Kane quantum computer architecture is shown in Fig. 1. The short description given here follows Goan and Milburn [18]. This architecture consists of ^{31}P atoms doped in a purified ^{28}Si ($I=0$) host. Each

*Electronic address: hillcd@physics.uq.edu.au
†Mailing address: Center for Quantum Computer Technology, C/– Department of Physics, The University of Queensland, St. Lucia, QLD 4072, Australia. Electronic address: goan@physics.uq.edu.au

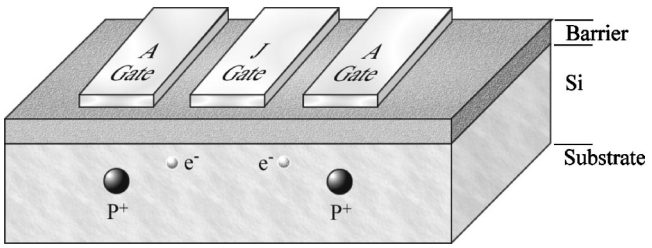

FIG. 1. The Kane quantum computer architecture.

P atom has nuclear spin of $I=\frac{1}{2}$. Electrodes placed directly above each P atom are referred to as A gates and those between atoms are referred to as J-gates. An oxide barrier separates the electrodes from the P-doped Si.

Each P atom has five valence electrons. As a first approximation, four of these electrons form covalent bonds with neighboring Si atoms, with the fifth forming a hydrogen-like S-orbital around each P^+ ion. This electron is loosely bound to the P donor and has a Bohr radius of $a_B^* \approx 3$ nm, allowing an electron mediated interaction between neighboring nuclei.

In this paper, nuclear-spin states will be represented by the states $|1\rangle$ and $|0\rangle$. Electronic spin states will be represented by $|\uparrow\rangle$ and $|\downarrow\rangle$. Where electronic states are omitted, it is assumed that they are polarized in the $|\downarrow\rangle$ state. *X*, *Y*, and *Z* are the Pauli matrices operating on electron and nuclear spins. That is,

$$X=\sigma_x, \quad Y=\sigma_y, \quad Z=\sigma_z. \tag{1}$$

Operations which may be performed on any system are governed by the Hamiltonian of the system. We now describe the effective spin Hamiltonian for two adjacent qubits of the Kane quantum computer and give a short physical motivation for each term which makes up the overall Hamiltonian

$$H=\sum_{i=1}^{2} H_{B_i}+H_{A_i}+H_J+H_{ac_i}, \tag{2}$$

where the summation is over each donor atom in the system *i*.

Under typical operating conditions, a constant magnetic field *B* will be applied to the entire system, perpendicular to the surface. This contributes Zeeman energies to the Hamiltonian

$$H_B=-g_n\mu_n BZ_n+\mu_B BZ_e. \tag{3}$$

A typical value for the Kane quantum computer of $B=2.0$ T gives Zeeman energy for the electrons of $\mu_B B \approx 0.116$ meV and for the nucleus $g_n\mu_n B \approx 7.1\times10^{-5}$ meV.

The hyperfine interaction couples between nuclear and electronic spins. The contribution of the hyperfine interaction to the Hamiltonian is

$$H_A=A\sigma_e\sigma_n, \tag{4}$$

where strength *A* of the hyperfine interaction is proportional to the value of the electron wave function evaluated at the nucleus

$$A=\frac{8\pi}{3}\mu_B g_n\mu_n|\psi(0)|^2. \tag{5}$$

A typical strength for the hyperfine interaction is $A=1.2\times10^{-4}$ meV. Charged A gates placed directly above each P nucleus distort the shape of the electronic wave function, thereby reducing the strength of the hyperfine coupling. The nature of this effect is under numerical investigation [29]. In this paper, we have assumed that it will be possible to vary the hyperfine coupling by up to $\approx 50\%$.

The exchange interaction couples adjacent electrons. Its contribution to the Hamiltonian is

$$H_J=J\sigma_{e_1}\sigma_{e_2}, \tag{6}$$

where e_1 and e_2 are two adjacent electrons. The magnitude *J* of the exchange interaction depends on the overlap of adjacent electronic wave functions. J gates placed between nuclei distort both electronic wave functions to increase or decrease the magnitude of this interaction. A typical value for the exchange energy is $4J=0.124$ meV, and in this paper, we assume that it will be possible to vary the magnitude of the exchange interaction from $J=0$ to $J\approx 0.043$ meV.

A rotating magnetic field, of strength B_{ac} rotating at a frequency of ω_{ac} can be applied, perpendicular to the constant magnetic field *B*. The contribution of the rotating magnetic field to the Hamiltonian is

$$\begin{aligned} H_{ac}=&-g_n\mu_n B_{ac}[X_n\cos(\omega_{ac}t)+Y_n\sin(\omega_{ac}t)] \\ &+\mu_B B_{ac}[X_e\cos(\omega_{ac}t)+Y_e\sin(\omega_{ac}t)], \end{aligned} \tag{7}$$

where the strength of the rotating magnetic field is envisioned to be $B_{ac}\approx 0.0025$ T.

At an operating temperature of $T=100$ mK, the electrons are almost all polarized by the magnetic field. That is,

$$\frac{n_e^{\uparrow}}{n_e^{\downarrow}}\approx 2.14\times10^{-12}. \tag{8}$$

We assume that electrons are polarized in the $|\downarrow\rangle$ state, and use nuclear-spin states as our computational basis.

B. Z rotations

Single-qubit rotations are required to implement the two-qubit gates described in this paper, as well as being essential for universality. In fact, as we will see they contribute significantly to the overall time and fidelity of each two-qubit gate. It is therefore important to consider the time required to implement *Z*, *X*, and *Y* rotations.

In this section we describe how fast *Z* rotations may be performed varying the voltage on the A gates only. A *Z* rotation is described by the equation

$$R_z(\theta)=e^{i\theta Z/2}. \tag{9}$$

TABLE I. Typical parameters for a Z rotation.

Description	Term	Value (meV)
Unperturbed hyperfine interaction	A	0.1211×10^{-3}
Hyperfine interaction during Z rotation	A_z	0.0606×10^{-3}

A z gate (phase flip) may be implemented as a rotation. It is given up to a global phase by

$$Z=-iR_z(\pi). \tag{10}$$

Under the influence of a constant magnetic field B to second order in A [18], each nuclei will undergo Larmor precession around the Z axis, at frequency of

$$\hbar\omega_l=2g_n\mu_nB+2A+\frac{2A^2}{\mu_BB+g_n\mu_nB}. \tag{11}$$

Z rotations may be performed by variation of the hyperfine interaction from A to A_z giving a difference in rotation frequency of

$$\hbar\omega_z=2(A-A_z)+\frac{2(A^2-A_z^2)}{\mu_BB+g_n\mu_nB}. \tag{12}$$

Perturbing the hyperfine interaction for one of the atoms and allowing free evolution, will rotate this atom with respect to the rotation of the unperturbed atoms. The speed of single atom Z rotations depends on how much it is possible to vary the strength of the hyperfine interaction A. For numerical simulation we use the typical values shown in Table I.

Under these conditions, a z gate may be performed on a single nuclear spin in approximately

$$t_Z\approx0.021\ \ \mu\text{s}. \tag{13}$$

These rotations occur in a rotating frame that precesses around the Z axis with a frequency equal to the Larmor frequency. We may have to allow a small time of free evolution until nuclei that are not affected by the Z rotation orient themselves to their original phase. The time required for this operation is less than

$$t_F\leqslant0.02\ \ \mu\text{s}. \tag{14}$$

C. *X* and *Y* rotations

In this section, we show how techniques, similar to those used in NMR (nuclear magnetic resonance) [18,30,31], may be used to implement X and Y rotations. X and Y rotations are described by the equations

$$R_x(\theta)=e^{i\theta X/2}, \tag{15}$$

$$R_y(\theta)=e^{i\theta Y/2}. \tag{16}$$

TABLE II. Typical parameters for an X rotation.

Description	Term	Value
Unperturbed hyperfine interaction	A	0.1211×10^{-3} meV
Hyperfine interaction during X rotation	A_x	0.0606×10^{-3} meV
Constant magnetic-field strength	B	2.000 T
Rotating magnetic-field strength	B_{ac}	0.0025 T

X and Y rotations are performed by application of a rotating magnetic field B_{ac}. The rotating magnetic field is resonant with the Larmor precession frequency given in Eq. (11), that is,

$$\omega_{ac}=\omega_l. \tag{17}$$

In contrast to NMR, in the Kane proposal we have direct control over the Larmor frequency of each individual P nucleus. By reducing the hyperfine coupling for the atom, we wish to target from A to A_x, we may apply an oscillating magnetic field that is only resonant with the Larmor frequency of only one of the atoms. This allows us to induce an X or Y rotation on an individual atom. To the first order, the frequency of this rotation may be approximated by

$$\hbar\omega_x=g_n\mu_nB_{ac}\left(1+\frac{A_x}{g_n\mu_nB}\right). \tag{18}$$

The speed of an X rotation is directly proportional to the strength of the rotating magnetic field B_{ac}. As the strength of the rotating magnetic field B_{ac} increases, the fidelity of the operation decreases. The reason is that in frequency space the full width at half maximum of the transition excited by the rotating magnetic field increases in proportion to B_{ac}. That is, as B_{ac} increases, we begin to excite nonresonant transitions. The larger separation, in frequency space, between Larmor frequencies, the smaller this systematic error. Since the Larmor precession frequency depends on how much we are able to vary the hyperfine interaction A, it determines how strong we are able to make B_{ac}.

For the purpose of simulation, the typical values shown in Table II for the unperturbed hyperfine interaction strength A, the hyperfine interaction strength during the X rotation A_x, applied magnetic-field strength B, and rotating magnetic-field strength B_{ac} were used.

Using these parameters, this gives the overall time to perform an X gate on a single-qubit in approximately

$$t_X\approx6.4\ \ \mu\text{s}. \tag{19}$$

Any single-qubit gate may be expressed as a product of X, Y and Z rotations. Ideally, X and Y rotations should be minimized because Z rotations may be performed much faster than X or Y rotations. For example, a Hadamard gate may be expressed as a product of Z and X rotations:

$$H=R_z\left(\frac{\pi}{2}\right)R_x\left(\frac{\pi}{2}\right)R_z\left(\frac{\pi}{2}\right). \tag{20}$$

Thus, from the above discussion, the Hadamard gate takes a time of approximately

$$t_H \approx 3.2 \ \ \mu\text{s}. \tag{21}$$

D. Nuclear-spin interaction

In this section, we show the results of second order perturbation theory to describe the interaction between two neighboring P atoms. This interaction between nuclei is coupled by electron interactions. We consider the case where the hyperfine couplings between each nucleus and its electron are equal, that is,

$$A = A_1 = A_2. \tag{22}$$

We allow coupling between electrons, that is,

$$J > 0, \tag{23}$$

but restrict ourselves to be far from an electronic energy-level crossing

$$J \ll \frac{\mu_B B}{2}. \tag{24}$$

Under these conditions electrons will remain in the polarized $|\downarrow\downarrow\rangle$ ground state.

In this situation, analysis has been performed using the second-order perturbation theory [18]. To second order in A, the energy levels are

$$E_{|11\rangle} = -2\mu_B B + J + 2g_n\mu_n B + 2A, \tag{25}$$

$$E_{|s_n\rangle} = -2\mu_B B + J - \frac{2A^2}{\mu_B B + g_n\mu_n B}, \tag{26}$$

$$E_{|a_n\rangle} = -2\mu_B B + J - \frac{2A^2}{\mu_B B + g_n\mu_n B - 2J}, \tag{27}$$

$$E_{|00\rangle} = -2\mu_B B + J - 2g_n\mu_n B - 2A - \frac{2A^2}{\mu_B B + g_n\mu_n B - 2J} - \frac{2A^2}{\mu_B B + g_n\mu_n B}, \tag{28}$$

where the symmetric $|s_n\rangle$ and antisymmetric $|a_n\rangle$ energy eigenstates are given by

$$|s_n\rangle = \frac{1}{\sqrt{2}}(|10\rangle + |01\rangle), \tag{29}$$

$$|a_n\rangle = \frac{1}{\sqrt{2}}(|10\rangle - |01\rangle). \tag{30}$$

Notice that the energies are symmetric around

$$E_0 = -2\mu_B B + J - \frac{A^2}{\mu_B B + g_n\mu_n B - 2J} - \frac{A^2}{\mu_B B + g_n\mu_n B}. \tag{31}$$

TABLE III. Typical parameters during interaction.

Description	Term	Value (meV)
Hyperfine interaction during interaction	A_U	0.1197×10^{-3}
Exchange interaction during interaction	J_U	0.0423

Since we are free to choose our zero-point energy to be E_0 (or equivalently ignore a global phase of a wave function $|\psi\rangle$) we may rewrite the second-order approximation as

$$E_{|\downarrow\downarrow\rangle|11\rangle} = \hbar\omega_B, \tag{32}$$

$$E_{|\downarrow\downarrow\rangle|s_n\rangle} = \hbar\omega_S, \tag{33}$$

$$E_{|\downarrow\downarrow\rangle|a_n\rangle} = -\hbar\omega_S, \tag{34}$$

$$E_{|\downarrow\downarrow\rangle|00\rangle} = -\hbar\omega_B, \tag{35}$$

where ω_B and ω_S are given by

$$\hbar\omega_B = 2A + 2g_n\mu_n B + \frac{A^2}{\mu_B B + g_n\mu_n B} + \frac{A^2}{\mu_B B + g_n\mu_n B - 2J}, \tag{36}$$

$$\hbar\omega_S = \frac{A^2}{\mu_B B + g_n\mu_n B - 2J} - \frac{A^2}{\mu_B B + g_n\mu_n B}. \tag{37}$$

The reason for this representation of the energy will become clear in the following section. Typical values used during numerical simulation of the interaction between nuclei are shown in Table III.

III. THE CANONICAL DECOMPOSITION

In this section, we describe the canonical decomposition and describe how this decomposition may be applied to the Kane quantum computer.

A. Mathematical description of canonical decomposition

The canonical decomposition [25,27] decomposes any two-qubit unitary operator into a product of four single-qubit unitaries and one entangling unitary:

$$U = (V_1 \otimes V_2) U_{can} (W_1 \otimes W_2), \tag{38}$$

where V_1, V_2, W_1, and W_2 are single-qubit unitaries, and U_{can} is the two-qubit interaction. The symbol $\otimes$ represents the tensor product of two matrices.

U_{can} has a simple form involving only three parameters, α_x, α_y, and α_z:

$$U_{can} = e^{i\alpha_x X\otimes X} e^{i\alpha_y Y\otimes Y} e^{i\alpha_z Z\otimes Z}. \tag{39}$$

This purely nonlocal term is known as the *interaction content* of the gate. It is not difficult to show that each of the terms in the interaction content, $e^{i\alpha_x X\otimes X}$, $e^{i\alpha_y Y\otimes Y}$, and $e^{i\alpha_z Z\otimes Z}$, commute with each other.

Physically each of the terms $e^{i\alpha_x X\otimes X}$, $e^{i\alpha_y Y\otimes Y}$, and $e^{i\alpha_z Z\otimes Z}$ correspond to a type of controlled rotation. For example, following Ref. [28],

$$\begin{aligned} e^{i\alpha_z Z\otimes Z} &= \cos\alpha_z I\otimes I + i\sin\alpha_z Z\otimes Z \\ &= \cos\alpha_z(|0\rangle\langle 0| + |1\rangle\langle 1|)\otimes I \\ &\quad + i\sin\alpha_z(|0\rangle\langle 0| - |1\rangle\langle 1|)\otimes Z \\ &= |0\rangle\langle 0|\otimes e^{i\alpha_z Z} + |1\rangle\langle 1|\otimes e^{-i\alpha_z Z} \\ &= (I\otimes e^{i\alpha_z Z})(|0\rangle\langle 0|\otimes I + |1\rangle\langle 1|\otimes e^{-i2\alpha_z Z}). \end{aligned} \tag{40}$$

This shows that up to a single-qubit rotation, $e^{i\alpha_z Z\otimes Z}$ is equivalent to a controlled Z rotation. This holds true for the other two terms. If we denote the eigenstates of X by

$$X|x_+\rangle = +|x_+\rangle, \tag{41}$$

$$X|x_-\rangle = -|x_-\rangle, \tag{42}$$

then a similar analysis shows that

$$(I\otimes e^{-i\alpha_x X})e^{i\alpha_x X\otimes X} = |x_+\rangle\langle x_+|\otimes I + |x_-\rangle\langle x_-|\otimes e^{-i2\alpha_x X}, \tag{43}$$

and that

$$(I\otimes e^{-i\alpha_y Y})e^{i\alpha_y Y\otimes Y} = |y_+\rangle\langle y_+|\otimes I + |y_-\rangle\langle y_-|\otimes e^{-i2\alpha_y Y}. \tag{44}$$

These operations are equivalent to controlled rotations in the X and Y directions, respectively. For the first case, if the control qubit is in the $|x_-\rangle$ state an X rotation is applied to the target qubit, and not applied if the control qubit is in the $|x_+\rangle$ state. Similarly for Y.

Single-qubit rotations, V_1, V_2, W_1, W_2, are possible on the Kane quantum computing architecture, the remaining task is to specify the pulse sequence for the purely entangling unitary U_{can}. Fortunately, this is always possible, as *any* interaction (with single-qubit rotations) between the two nuclei is sufficient [32]. In fact, it is a relatively simple task to use almost any interaction between qubits to generate any desired operation.

B. Calculation of the interaction content between nuclei

In this section, we will see how it is possible to apply the canonical decomposition to the Kane quantum computer. This is important as this natural interaction of the system will be manipulated by single-qubit unitaries to find the pulse scheme of any two-qubit gate. The canonical decomposition provides a unique way of looking at this interaction.

The interaction that we will apply the canonical decomposition to is free evolution of the configuration described in Sec. II D, using the results cited there from the second-order perturbation theory. After a particular time of free evolution, our system will have evolved according to unitary dynamics, which we may decompose using the canonical decomposition:

$$U_{sys} = (V_1^s\otimes V_2^s)U_{can}^s(W_1^s\otimes W_2^s), \tag{45}$$

where the superscript s indicates a physical operation present in our *system*.

We wish to find the interaction content U_{can}^s of this free evolution. Systematic methods for doing this are given in Refs. [25,26,33]. This is most easily done by noting any interaction content, U_{can} is diagonal in the so-called magic basis, otherwise known as the Bell basis. This basis is

$$|\Phi_1\rangle = \frac{1}{\sqrt{2}}(|00\rangle + |11\rangle), \tag{46}$$

$$|\Phi_2\rangle = \frac{-i}{\sqrt{2}}(|00\rangle - |11\rangle), \tag{47}$$

$$|\Phi_3\rangle = \frac{1}{\sqrt{2}}(|01\rangle - |10\rangle), \tag{48}$$

$$|\Phi_4\rangle = \frac{-i}{\sqrt{2}}(|01\rangle + |10\rangle). \tag{49}$$

α_x, α_y, and α_z are related to the eigenvalues $e^{i\lambda_1}$, $e^{i\lambda_2}$, $e^{i\lambda_3}$, and $e^{i\lambda_4}$ of U_{can}. That is,

$$\lambda_1 = +\alpha_x - \alpha_y + \alpha_z, \tag{50}$$

$$\lambda_2 = -\alpha_x + \alpha_y + \alpha_z, \tag{51}$$

$$\lambda_3 = -\alpha_x - \alpha_y - \alpha_z, \tag{52}$$

$$\lambda_4 = +\alpha_x + \alpha_y + \alpha_z. \tag{53}$$

It is possible to relate these eigenvalues to our system. After a time t, each of the eigenstates of the system will have evolved according the Schrödinger equation, which we may view as having performed an operation $U_{sys}(t)$ on the system. As we showed in Sec. II D

$$U_{sys}|11\rangle = e^{+i\theta_B}|11\rangle, \tag{54}$$

$$U_{sys}|00\rangle = e^{-i\theta_B}|00\rangle, \tag{55}$$

$$U_{sys}|s\rangle = e^{+i\theta_S}|s\rangle, \tag{56}$$

$$U_{sys}|a\rangle = e^{-i\theta_S}|a\rangle, \tag{57}$$

where

$$\theta_S = \omega_S t, \tag{58}$$

$$\theta_B = \omega_B t. \tag{59}$$

Applying Eqs. (54)–(57) to Eqs. (46)–(49), we obtain

$$U_{sys}|\Phi_1\rangle = \cos(\theta_B)|\Phi_1\rangle - \sin(\theta_B)|\Phi_2\rangle, \tag{60}$$

$$U_{sys}|\Phi_2\rangle = \cos(\theta_B)|\Phi_2\rangle + \sin(\theta_B)|\Phi_1\rangle, \tag{61}$$

$$U_{sys}|\Phi_3\rangle = e^{-i\theta_S}|\Phi_3\rangle, \tag{62}$$

$$U_{sys}|\Phi_4\rangle = e^{+i\theta_S}|\Phi_4\rangle. \tag{63}$$

This shows that in the magic basis, U_{sys} is given by

$$U_{sys} = \begin{bmatrix} \cos(\theta_B) & \sin(\theta_B) & 0 & 0 \\ -\sin(\theta_B) & \cos(\theta_B) & 0 & 0 \\ 0 & 0 & e^{-i\theta_S} & 0 \\ 0 & 0 & 0 & e^{i\theta_S} \end{bmatrix}. \tag{64}$$

It is possible to find the eigenvalues λ_1, λ_2, λ_3, and λ_4. We note that the eigenvalues of $U^T U$ in the magic basis are given by

$$\lambda(U^T U) = \{e^{2i\lambda_1}, e^{2i\lambda_2}, e^{2i\lambda_3}, e^{2i\lambda_4}\}. \tag{65}$$

Calculation of the eigenvalues of $U_{sys}^T U_{sys}$ is easy since $U_{sys}^T U_{sys}$ is already diagonal in this basis, with diagonal elements being $\{1,1,e^{-2i\theta_S}, e^{2i\theta_S}\}$. Care must be exercised at this point because it is not clear which branch should be used when taking the argument. In our case, as long as $0 \leqslant \theta_S \leqslant (\pi/2)$ [33], then

$$\lambda_1 = 0, \tag{66}$$

$$\lambda_2 = 0, \tag{67}$$

$$\lambda_3 = -\theta_S, \tag{68}$$

$$\lambda_4 = +\theta_S. \tag{69}$$

Using Eqs. (50)–(53) we may solve for the coefficients α_x, α_y, and α_z, giving

$$\alpha_x^s = \frac{1}{2}\theta_S, \tag{70}$$

$$\alpha_y^s = \frac{1}{2}\theta_S, \tag{71}$$

$$\alpha_z^s = 0. \tag{72}$$

Single-qubit rotations, W_1^s, W_2^s, V_1^s, V_2^s, induced are Z rotations. Z rotations are fast and may be canceled in comparatively less time by single-qubit Z rotations in the opposite direction:

$$(V_1^{s\dagger} \otimes V_2^{s\dagger}) U_{sys} (W_1^{s\dagger} \otimes W_2^{s\dagger}) = U_{can}^s. \tag{73}$$

For notational convenience, we will now label the interaction content of the system by an angle rather than by its time. The time for this interaction may be calculated through Eqs. (70)–(72), (58), and (37). Therefore, we write

$$U_{can}^s(\phi) = e^{i\phi X\otimes X + i\phi Y\otimes Y}, \tag{74}$$

where

$$\phi = \frac{1}{2}\theta_S. \tag{75}$$

This analysis has been based on the second order perturbation theory. As we approach the electronic energy-level crossing, this approach is no longer valid. Close to this crossing numerical analysis shows the eigenvalues are no longer symmetric which implies α_z^s becomes nonzero. Unfortunately, in this regime, we excite the system into higher-energy electronic configurations.

Given any two-qubit gate, such as the CNOT gate, there are many different possible choices of single-qubit rotations and free evolution that will implement a desired gate. Z rotations are faster single-qubit rotations than X and Y rotations, and therefore, it is desirable to minimize X and Y rotations in order to optimize the time required, for any given two-qubit gate.

IV. THE CNOT AND CONTROLLED Z GATES

A. Introduction

The CNOT gate is a particularly often cited example of a two-qubit gate. CNOT and single-qubit rotations are universal for quantum computation [34]. Many implementations, including the Kane proposal [9], use this fact to demonstrate that they can, in principle, perform any quantum algorithm. It is a member of the so-called fault tolerant [35] set of gates, which are universal for quantum computing, and are particularly important in error correction. In this section, we find a pulse scheme to implement the CNOT gate on the Kane quantum computer.

Controlled Z rotations, sometimes known as controlled phase gates, are some of the most important operations for implementing quantum algorithms. In particular, one of the simplest ways to implement quantum Fourier transformations uses multiple controlled Z rotations (see, for example, Ref. [36]). Single-qubit rotations and the controlled Z gate are, like the CNOT gate, universal for quantum computation. Controlled Z rotations may be used in the construction of controlled X and Y rotations. In this section we find a pulse scheme to implement any controlled Z rotation on the Kane quantum computer.

Because these two gates have similar interaction contents, we consider them together. We will first show how to construct a controlled-Z gate of any angle and use this gate directly to construct a CNOT gate.

A controlled Z rotation of angle θ is defined in the computational basis by

$$U_{\Lambda Z}(\theta) = \begin{bmatrix} 1 & 0 & 0 & 0 \\ 0 & 1 & 0 & 0 \\ 0 & 0 & 1 & 0 \\ 0 & 0 & 0 & e^{i\theta} \end{bmatrix}. \tag{76}$$

The canonical decomposition of the controlled Z rotation by an angle θ has an interaction content consisting of

$$\alpha_x = 0, \tag{77}$$

$$\alpha_y = 0, \tag{78}$$

$$\alpha_z = \frac{\theta}{2}. \tag{79}$$

This interaction content may be found by using systematic methods [25,26,33]. The controlled-Z gate also requires a Z rotation as described by Eq. (40).

CNOT is defined in the computational basis by the matrix

$$U_{\mathrm{CNOT}} = \begin{bmatrix} 1 & 0 & 0 & 0 \\ 0 & 1 & 0 & 0 \\ 0 & 0 & 0 & 1 \\ 0 & 0 & 1 & 0 \end{bmatrix}. \tag{80}$$

The canonical decomposition of CNOT has an interaction content with angles of

$$\alpha_x = 0, \tag{81}$$

$$\alpha_y = 0, \tag{82}$$

$$\alpha_z = \frac{\pi}{4}. \tag{83}$$

Since the CNOT and controlled-Z gates are both types of controlled rotation similar to those described in Sec. III A, it is not a surprise that they have a similar interaction content. In fact, control-Z gates (that is, a controlled Z rotation by an angle of π) and CNOT gates have an identical interaction content, and are therefore equivalent up to single-qubit rotations. A CNOT gate may be constructed from a control-Z gate conjugated by $I \otimes H$.

B. The construction

Our first task in finding a suitable pulse scheme for the controlled Z rotation is to find a pulse scheme which implements the interaction content [Eqs. (77)–(79)] of the controlled Z rotation. Techniques have direct analogs in NMR [30,31].

The first technique [28] is to conjugate by $I \otimes X$, $I \otimes Y$, or $I \otimes Z$ to change the sign of two of these parameters. For example,

$$(I \otimes Z) e^{i\alpha_x X \otimes X + i\alpha_y Y \otimes Y + i\alpha_z Z \otimes Z} (I \otimes Z) = e^{-i\alpha_x X \otimes X - i\alpha_y Y \otimes Y + i\alpha_z Z \otimes Z}. \tag{84}$$

This can be useful because it allows us to exactly cancel every controlled rotation except one

$$(I \otimes Z) U_{can} (I \otimes Z) U_{can} = e^{i2\alpha_z Z \otimes Z}. \tag{85}$$

In our case, however, it turns out that $\alpha_z^s = 0$. In order to reorder the parameters, a useful technique is to conjugate by Hadamardgates [28]. This is one of only several choices of single-qubit rotations which reorder the parameters. In this case, the order of the parameters is

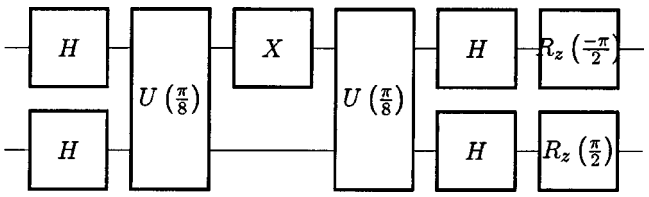

FIG. 2. Circuit diagram for controlled Z pulse sequence.

$$(H \otimes H) e^{i\alpha_x X \otimes X + i\alpha_y Y \otimes Y + i\alpha_z Z \otimes Z} (H \otimes H) = e^{i\alpha_z X \otimes X + i\alpha_y Y \otimes Y + i\alpha_x Z \otimes Z}. \tag{86}$$

Combining these two techniques gives the following construction:

$$e^{i\theta Z \otimes Z} = (Z \otimes I)(H \otimes H) U_{can}^{s}\left(\frac{\theta}{2}\right)(H \otimes H)(Z \otimes I) \times (H \otimes H) U_{can}^{s}\left(\frac{\theta}{2}\right)(H \otimes H). \tag{87}$$

To find the final construction, several one-qubit optimizations were made by combining adjacent single-qubit rotations and using the identities

$$HZH = X, \tag{88}$$

$$HH = I. \tag{89}$$

Operations may be performed in parallel. For example, performing identical X or Y rotations on separate nuclei is a natural operation of the system because magnetic fields are applied globally. Performing operations in parallel is faster and also have higher fidelity than performing them one at a time.

The construction of the controlled Z rotation is shown in Fig. 2. In this circuit, the single-qubit rotations specified in Eq. (40) have been included. The period of interaction between nuclei may be increased or decreased to produce controlled rotations by any angle θ as specified in Eqs. (87), (74), (58), and (37).

Our task of constructing a CNOT gate is now comparatively simple. We note that a CNOT gate has the same interaction term as the controlled-Z (controlled phase) operation. These gates are therefore equivalent up to local operations.

Conjugation by $I \otimes H$ will turn a controlled-Z operation into a CNOT gate. Using some simple one qubit identities to simplify the rotations at the beginning and end of the pulse sequences, we arrive at the decomposition illustrated in the circuit diagram shown in Fig. 3.

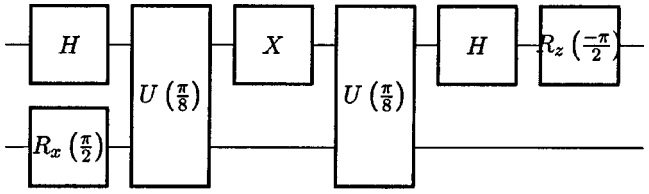

FIG. 3. Circuit diagram for the CNOT pulse sequence.

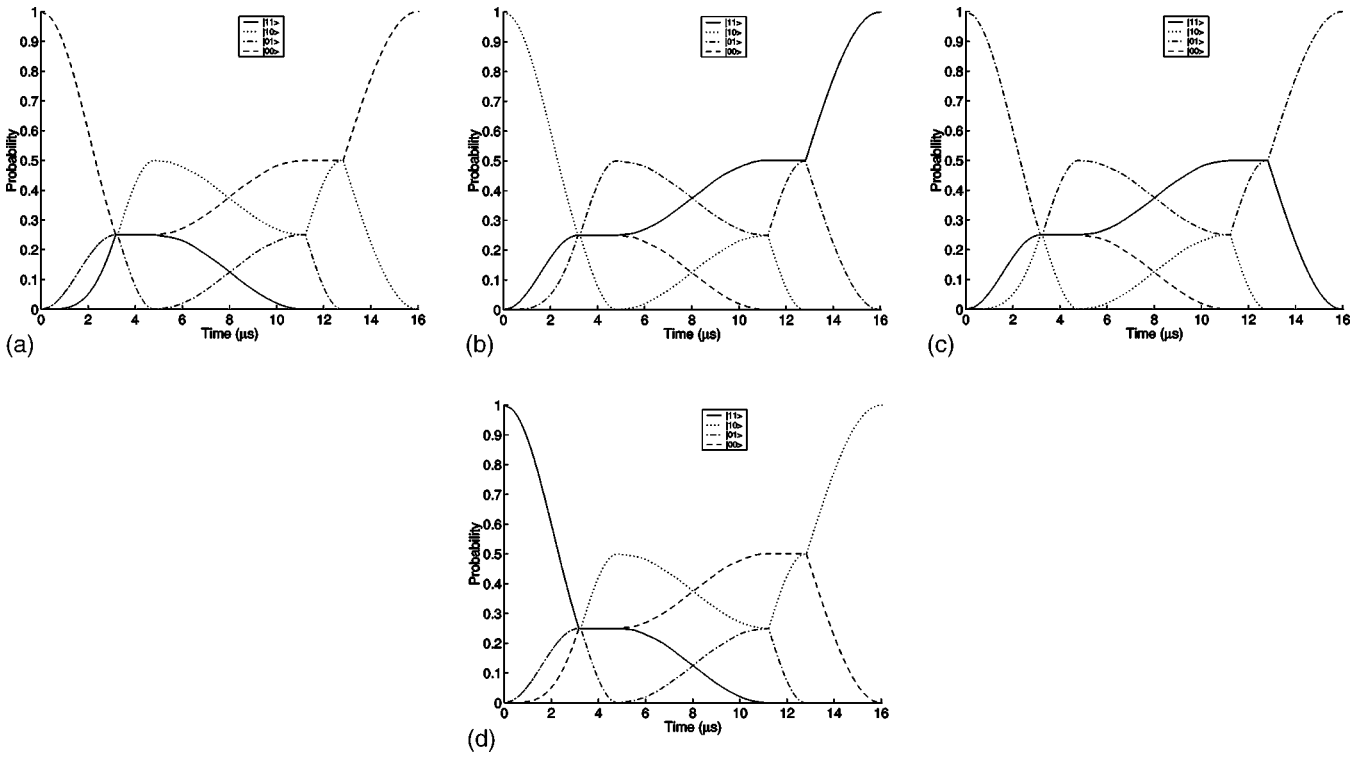

FIG. 4. Numerical simulation of the CNOT gate showing different initial conditions.

C. Time and fidelity

Throughout the paper, we define fidelity as

$$F(|\psi\rangle,|\psi_0\rangle)=|\langle\psi|\psi_0\rangle|^2, \tag{90}$$

with $|\psi\rangle$ being the actual state obtained from evolution and $|\psi_0\rangle$ being the state which is desired. We define the error in terms of the fidelity as

$$E=\max_{|\psi\rangle}[1-F(|\psi\rangle,|\psi_0\rangle)], \tag{91}$$

where the maximization is performed over the output of all the computational basis states $|\psi\rangle$.

Numerical simulations were carried out by numerically integrating Schrödinger's equation for the Hamiltonian of the system, Eq. (2). The results of this numerical simulation for the pulse sequence of the CNOT gate are shown in Fig. 4. These graphs show each of the states and the transitions which are made. In these figures, it is possible to see the evolution of each of the four computational basis states. The control qubit is the second qubit and the target qubit is the first qubit.

According to the numerical results, a full controlled-Z gate takes a total time of 16.1 μs and has an error of $\approx 4\times10^{-5}$. Similarly, we find the CNOT gate takes a total time of 16.0 μs. The time required for this gate can be grouped as shown in Table IV.

X and *Y* rotations make up the majority of the time taken to implement the controlled-Z and CNOT gates. In the CNOT gate, only 3.2 μs is spent implementing the entangling part of the gate, whereas 12.6 μs is required to implement the *X* and *Y* rotations.

We can see via simulation that the systematic error in the CNOT gate is $\approx 4\times10^{-5}$. Some of these error will be due to errors during simulation and breakdown of the second-order approximation. A large part of the error, particularly if the hyperfine interaction may not be varied very much, is due to *X* rotations where unintended nonresonant transitions are excited along with the intended rotation.

V. THE SWAP AND SQUARE ROOT OF SWAP GATES

A. Introduction

One of the most important gates for the Kane quantum computer is envisioned to be the swap gate. This is because, in the Kane proposal, only nearest-neighbor interactions are allowed. This gate swaps the quantum state of two-qubits. By using the swap gate it is possible to swap qubits until they are the nearest neighbors, interact with them, and then swap them back again. Having an efficient method to interact qubits which are not adjacent to each other is therefore im-

TABLE IV. Time for the CNOT gate.

Description	Time μs
X rotations	12.6
Z rotations	0.2
Two qubit interaction	3.2
Total	16.0

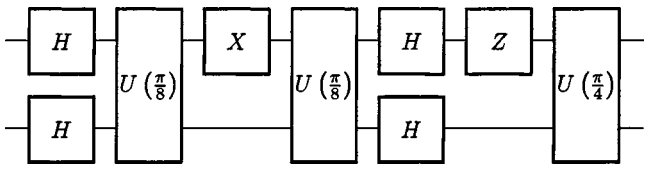

FIG. 5. Circuit diagram for the swap gate pulse sequence.

portant, and the swap gate, with its high level of information transfer, is one possible method of achieving this.

The square root of swap gate has been suggested for the quantum-dot-spin based quantum computer architecture [37], where it is a particularly natural operation. In our system, it is not such a natural operation, but that does not mean that we cannot construct it. Like the CNOT gate, the square root of swap (together with single-qubit rotations) is universal for quantum computation. In this section, we find a pulse sequence to implement both the swap and the square root of swap gates on the Kane quantum computer architecture.

The swap gate is defined in the computational basis by

$$U_{swap}=\begin{bmatrix}1&0&0&0\\0&0&1&0\\0&1&0&0\\0&0&0&1\end{bmatrix}. \tag{92}$$

The canonical decomposition of the swap gate has an interaction content with angles of

$$\alpha_x=\frac{\pi}{4}, \tag{93}$$

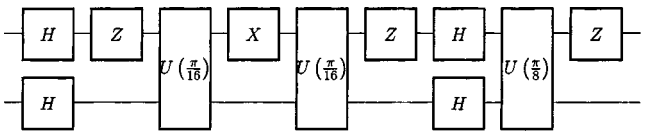

FIG. 6. The circuit diagram for the square root of the swap pulse sequence.

$$\alpha_y=\frac{\pi}{4}, \tag{94}$$

$$\alpha_z=\frac{\pi}{4}. \tag{95}$$

The square root of the swap gate is defined in the computational basis by

$$U_{SS}=\begin{bmatrix}1&0&0&0\\0&\frac{1}{2}(1+i)&\frac{1}{2}(1-i)&0\\0&\frac{1}{2}(1-i)&\frac{1}{2}(1+i)&0\\0&0&0&1\end{bmatrix}. \tag{96}$$

The canonical decomposition of the square root of the swap gate has an interaction term consisting of

$$\alpha_x=-\frac{\pi}{8}, \tag{97}$$

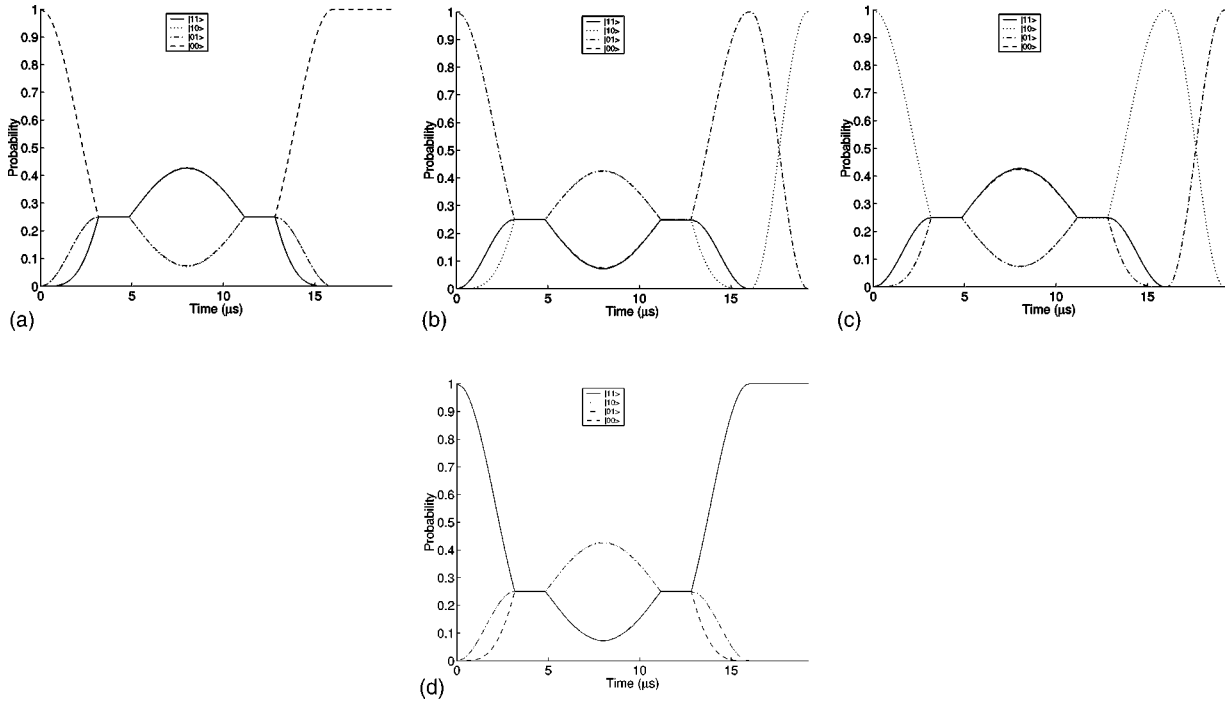

FIG. 7. Numerical simulation of the swap gate.

TABLE V. Gate times and fidelities.

Gate	Time (μs)	Error
CNOT	16.0	4×10^{-5}
Swap	19.2	7×10^{-5}
Square root of swap	16.2	5×10^{-5}
Controlled z	16.1	4×10^{-5}

$$\alpha_y = -\frac{\pi}{8}, \tag{98}$$

$$\alpha_z = -\frac{\pi}{8}. \tag{99}$$

Since the square root of swap and swap gates have essentially the same interaction content, their constructions are very similar, and are therefore considered together here.

B. The construction

The easiest way to construct a swap gate is simply to use free evolution to obtain the angles α_x and α_y which is natural for our system. The only remaining term is the α_z term, which for our system will naturally be zero. We may obtain this term by applying a pulse sequence similar to the controlled Z rotation as described in Sec. IV. The resulting construction swap gate is shown in the diagram in Fig. 5.

The interaction content of the square root of swap gate is exactly half that of the swap gate, and it is negative. We use exactly the same technique used to obtain the swap gate, only allowing the nuclei to interact for exactly half the time. To make the terms negative, we conjugate by $Z\otimes I$. The construction of the square root of swap gate obtained using this method is shown in Fig. 6.

C. Speed and fidelity

The swap and square root of swap gates were simulated numerically. The resulting transitions for the swap gate are shown in Fig. 7. Similar results were obtained for the square root of swap gate, not shown here.

The swap gate takes a total time of 19.2 μs, and has a fidelity of $\approx 7\times10^{-5}$. The majority of time in this gate is taken by X and Y rotations, which are also the major sources of error.

This is substantially faster than an existing suggestion for the swap gate [19] of 192 μs. It is also faster than using three adiabatic CNOT gates, which would take ≈ 78 μs.

According to numerical simulation the square root of swap gate takes 16.8 μs and has an error of approximately 5×10^{-5}. This is the first explicit proposal for the Kane quantum computer for the square root of swap gate.

The square root of swap gate has been suggested in the context of quantum computation for quantum dots [37]. It is universal for quantum computation and therefore can be used to construct a CNOT gate. Unfortunately in this case, a CNOT constructed from the square root of swap gate presented here would take approximately 40 μs which is much longer than the pulse sequence presented in this paper for the CNOT gate.

VI. CONCLUSION

We have shown how the canonical decomposition may be applied to the Kane quantum computer. We found the canonical decomposition of a natural operation of the computer, that is, free evolution with hyperfine interactions equal and the exchange interaction non-zero. We then used this interaction to form two-qubit gates which may be applied to the Kane quantum computer. These gates and their times and fidelities are shown in Table V.

The majority of the time required to implement each of these two-qubit gates is used to implement single-qubit rotations. Were we able to perform these rotations faster and more accurately then the gates presented here would also benefit. Another possible avenue of research is to investigate the effect of decoherence on the system.

To our knowledge, this is the fastest proposal for swap, square root of swap, CNOT, and controlled-Z operations on the Kane quantum computer architecture. We have shown how a representative set of two-qubit gates may be implemented on the Kane quantum computer. These methods may prove particularly powerful because they only involve characterization by three parameters which may be determined theoretically, as shown here, or through experiment. Once determined, these parameters may be used to construct *any* two-qubit gate.

ACKNOWLEDGMENTS

We would like to thank Gerard Milburn for support. C.D.H. would like to thank Mick Bremner, Jennifer Dodd, Henry Haselgrove, and Tobias Osborne for help and advice. H.S.G. would like to acknowledge financial support from Hewlett-Packard.

[1] L.K. Grover, Phys. Rev. Lett. **79**, 325 (1997).
[2] P.W. Shor, SIAM J. Comput. **26**, 1484 (1997).
[3] E. Knill, R. Laflamme, and G.J. Milburn, Nature (London) **409**, 46 (2001).
[4] N.A. Gershenfeld and I.L. Chuang, Science **275**, 350 (1997).
[5] D.G. Cory, A.F. Fahmy, and T.F. Havel, Proc. Natl. Acad. Sci. U.S.A. **94**, 1634 (1997).
[6] J.I. Cirac and P. Zoller, Phys. Rev. Lett. **74**, 4091 (1995).
[7] Y. Nakamura, Y.A. Pashkin, and J.S. Tsai, Nature (London) **398**, 786 (1998).
[8] A. Imamoglu, D.D. Awschalom, G. Burkard, D.P. DiVincenzo, D. Loss, M. Sherwin, and A. Small, Phys. Rev. Lett. **83**, 4204 (1999).
[9] B.E. Kane, Nature (London) **393**, 133 (1998).

[10] A. Honig, Phys. Rev. **96**, 254 (1954).
[11] J.P. Gordon and K.D. Bowers, Phys. Rev. Lett. **1**, 10 (1958).
[12] G. Feher and E.A. Gere, Phys. Rev. **114**, 1245 (1959).
[13] G. Feher, Phys. Rev. **114**, 1219 (1959).
[14] A. Honig and E. Stupp, Phys. Rev. **117**, 69 (1960).
[15] R.A. Faulkner, Phys. Rev. **184**, 713 (1969).
[16] M. Chiba and A. Hirai, J. Phys. Soc. Jpn. **33**, 730 (1972).
[17] J.S. Waugh and C.P. Slichter, Phys. Rev. B **37**, 4337 (1988).
[18] H.-S. Goan and G.J. Milburn (unpublished).
[19] C.J. Wellard, P.h.D. thesis, University of Melbourne, 2001 (unpublished).
[20] C.J. Wellard and L.C.L. Hollenberg, e-print quant-ph/0104055.
[21] A.G. Fowler, C.J. Wellard, and L.C.L. Hollenberg, Phys. Rev. A **67**, 012301 (2003).
[22] H.K. Cummins and J.A. Jones, New J. Phys. **2**, 6 (2000).
[23] R. Tyco, Phys. Rev. Lett. **51**, 775 (1983).
[24] C.J. Wellard, L.C.L. Hollenberg, and H.C. Pauli, Phys. Rev. A **65**, 032303 (2002).
[25] B. Kraus and J.I. Cirac, Phys. Rev. A **63**, 062309 (2001).
[26] K. Hammerer, G. Vidal, and J.I. Cirac, Phys. Rev. Lett. **88**, 237902 (2002).
[27] N. Khaneja, R. Brockett, and S. Glaser, Phys. Rev. A **63**, 032308 (2001).
[28] M.J. Bremner, C.M. Dawson, J.L. Dodd, A. Gilchrist, A.W. Harrow, D. Mortimer, M.A. Nielsen, and T.J. Osborne, Phys. Rev. Lett. **89**, 247902 (2002).
[29] L. Kettle, H.-S. Goan, S.C. Smith, L.C.L. Hollenberg, C.I. Pakes, and C. Wellard (unpublished).
[30] E.D. Becker, *High Resolution NMR*, 3rd ed. (Academic Press, San Diego, 2000).
[31] C.P. Slichter, *Principles of Magnetic Resonance*, 3rd ed. (Springer-Verlag, Berlin, 1990).
[32] J.L. Dodd, M.A. Nielsen, M.J. Bremner, and R.T. Thew, Phys. Rev. A **65**, 040301 (2002).
[33] H. Haselgrove (private communication).
[34] D. DiVincenzo, Phys. Rev. A **51**, 1015 (1995).
[35] P.W. Shor, in *Proceedings of the 37th Annual Symposium on Foundations of Computer Science* (IEEE Computer Society Press, Los Alamitos, CA, 1996), pp. 56–65.
[36] M.A. Nielsen and I.L. Chuang, *Quantum Computation and Quantum Information*, 2nd ed. (Cambridge University Press, Cambridge, 2001).
[37] D. Loss and D.P. DiVincenzo, Phys. Rev. A **57**, 120 (1998).